Summary Report on the Neutronics Activities Performed by the U.S. Home Team as Part of the Blanket Design Task D202 in 1995

M.E. Sawan, H.Y. Khater, L.A. El-Guebaly

March 1996

UWFDM-1007

FUSION TECHNOLOGY INSTITUTE

UNIVERSITY OF WISCONSIN

MADISON WISCONSIN

ITER/US/95/IV-BL-15

Summary Report on the Neutronics Activities Performed by the US Home Team as Part of the Blanket Design Task D202 in 1995

M. E. Sawan, H. Y. Khater, and L. A. El-Guebaly

Fusion Technology Institute
University of Wisconsin-Madison
1500 Engineering Drive
Madison, WI 53706

April 1996

UWFDM-1007

Executive Summary

During the year 1995, the US home team performed design tasks in the neutronics and activation area as part of the blanket design D202. These included responding to specific requests by the Nuclear Analysis group in Garching. Two multigroup working libraries were generated based on the most recent FENDL nuclear data evaluation. These libraries were used by the JCT in neutronics calculations. Several neutronics calculations were performed in the early stage of the ITER interim design to provide guidance for the blanket design regarding the impact of blanket thickness on magnet radiation effects and vacuum vessel helium production. We provided a recommended set of safety factors that need to be applied to the one-dimensional results in the early stages of the design to account for gaps between adjacent blanket modules and uncertainties in modeling and nuclear data. Since no well defined magnet radiation limits were provided for ITER early in the year, we demonstrated the impact of such limits on the reactor size by performing several one-dimensional calculations. The results implied that there is an immediate need for well defined magnet radiation limits.

At the request of the magnet design group in the US home team, we calculated the nuclear heating profiles in the most recent cased TF coil design. We continued providing support to the JCT Nuclear Analysis group in performing one- and two-dimensional neutronics and shielding calculations for the ITER shielding blanket. Recommendations regarding the vacuum vessel thickness required for adequate magnet protection in the inboard side were made. Neutronics calculations have been performed to determine the nuclear heating distribution in the bolt and surrounding components to be used in the 2D thermal analysis.

The poloidal distribution of the neutron wall loading in the interim design of ITER has been determined using the 3D radiation transport Monte Carlo code MCNP. The detailed geometrical configuration of the ITER first wall and the plasma facing surface of the divertor cassette has been modeled in the calculation. The MCNP code was modified to sample source neutrons from the pointwise source distribution in the ITER plasma provided numerically by the San Diego JCT at 1600 mesh points. The peak inboard and outboard wall loadings are 0.95 and 1.25 MW/m^2, respectively. The peak neutron wall loadings in the divertor cassette are 0.556 and 0.16 MW/m^2, respectively.

Two-dimensional activation calculations have been performed to calculate the biological dose outside the machine. The detailed radial build at the reactor midplane as provided by the JCT was included in the model. The R-ϑ model used includes 10,096 mesh points. All impurities in the FW, blanket, VV and magnet were included. The calculations were performed for different pulsing scenarios provided by the JCT. The 2D activation calculation has been updated to include the inter-coil structure, cryostat and biological shield. The effect of adding these components in the model was to reduce the dose after shutdown in the space between the vacuum vessel and the cryostat by a factor of ~5. Recommendations regarding accessibility for maintenance in the area behind the VV, TF coils, and cryostat were made.

I. INTRODUCTION

During the year 1995, the US home team performed design tasks in the neutronics and activation area as part of the blanket design D202. These included responding to specific requests by the Nuclear Analysis group in Garching. These included generating multigroup working libraries based on the FENDL nuclear data evaluation, providing guidance for the blanket design regarding magnet shielding performance, and providing a recommended set of safety factors to be applied to the one-dimensional results. We also assessed the impact of magnet radiation limits on the reactor size and calculated the nuclear heating profiles in the TF coils. We continued providing support to the JCT Nuclear Analysis group in performing one- and two-dimensional neutronics and shielding calculations for the ITER shielding blanket. The poloidal distribution of the neutron wall loading in the interim design of ITER has been determined using the 3D radiation transport Monte Carlo code MCNP. Two-dimensional activation calculations have been performed to calculate the biological dose outside the machine. This report summarizes the neutronics and activation tasks performed during the year 1995 as part of the blanket design task D202.

II. MULTIGROUP WORKING LIBRARIES BASED ON FENDL

An updated working multigroup cross section library based on the most recent international fusion evaluated nuclear data library (FENDL) was generated. This library includes nuclear data for 39 elements and isotopes required for ITER neutronics calculations. The multigroup structure includes 175 neutron energy groups and 42 gamma energy groups. The library includes all nuclear responses of interest for the ITER design. The library was provided to the JCT and has been used in one-dimensional calculations along with the ONEDANT code. Because of the large memory space needed for two-dimensional calculations with the TWODANT code, we generated a 46 neutron - 21 gamma group library by collapsing the large library using the standard VITAMIN-E weight function. Test runs for the one-dimensional blanket model indicated that the results from the coarse group library are very close to those obtained using the original fine group library. This library was also provided to the JCT for use in neutronics calculations, particularly two-dimensional calculations.

III. IMPACT OF BLANKET THICKNESS ON MAGNET AND VV DAMAGE

Several one-dimensional calculations have been performed to provide guidance for the blanket designers regarding the impact of blanket thickness on magnet radiation effects and vacuum vessel helium production. The calculations have been performed for the outline design

using the most recent FENDL/E-1.0 library with 175 neutron and 42 gamma energy groups. The effect of increasing the blanket thickness by 5 and 10 cm was determined. 60% 316SS and 40% H_2O were assumed in the added zone. The results were given for the inboard region and normalized to 1 MW/m^2 wall loading and 3 MWa/m^2 fluence. The results are given in Table 1.

Table 1
Effect of Blanket Thickness on Magnet and VV Damage for the Outline Design

Added thickness (cm)	0	5	10
End-of-life fast neutron fluence (n/cm^2)	1.50×10^{17}	7.83×10^{16}	4.09×10^{16}
End-of-life insulator dose (Rads)	1.28×10^{8}	6.64×10^{7}	3.44×10^{7}
End-of-life Cu dpa	9.65×10^{-5}	5.05×10^{-5}	2.62×10^{-5}
Peak power density (mW/cm^3)	0.031	0.016	0.008
End-of-life He appm in VV	0.361	0.160	0.070

The results indicate that an additional 5 cm yields about a factor of 2 reduction in magnet and VV damage. A 10 cm addition gives about a factor of 4 damage reduction. The damage levels reported in the October design assessment meeting are higher than values for the outline design. The results for the outline design given in Table 1 were scaled in Table 2 to show the effect of adding 5 and 10 cm to the October blanket design. The results were presented to the JCT and home teams during the blanket review meeting held in Garching during the period 20-24 February 1995.

Table 2
Effect of Blanket Thickness on Magnet and VV Damage for the October 1994 Blanket Design

Added thickness (cm)	0	5	10
End-of-life fast neutron fluence (n/cm^2)	5.70×10^{17}	2.97×10^{17}	1.55×10^{17}
End-of-life insulator dose (Rads)	6.40×10^{8}	3.32×10^{8}	1.72×10^{8}
End-of-life Cu dpa	4.0×10^{-4}	2.1×10^{-4}	1.1×10^{-4}
Peak power density (mW/cm^3)	0.140	0.072	0.037
End-of-life He appm in VV	0.66	0.29	0.13

IV. RECOMMENDED SAFETY FACTORS

We provided a recommended set of safety factors that need to be applied to the one-dimensional results to account for gaps between adjacent blanket modules and uncertainties in modeling and nuclear data. Shielding calculations based on one-dimensional neutronics calculations do not include effects of assembly gaps between modules and toroidal arrangement of materials in the blanket and VV. The 1D results for magnet and VV damage should be increased by a safety factor to account for streaming in the assembly gaps, approximations in modeling, and uncertainties in nuclear data. During the CDA a safety factor of 3 was used. We performed detailed 3D calculations for the CDA design (it has a gap configuration similar to the current ITER EDA design) to verify the safety factor adopted. The 3D results with gaps were compared to the 3D results without gaps to determine the gap effect. The 3D results without gaps were compared to 1D results to determine the effect of modeling.

For magnet damage, a safety factor of 3 is adequate to account for 2 cm gaps and uncertainties in modeling and nuclear data. A safety factor of 6 should be used for the 4 cm gap. Higher safety factors should be used for VV/back plate damage due to the larger peaking from assembly gaps. Since the assembly gaps do not penetrate all the way to the magnet, the damage peaking is lower at the magnets. A list of the recommended safety factors is given in Table 3. These recommendations were presented to the JCT and home teams during the blanket review meeting held in Garching during the period 20-24 February 1995.

Table 3
Recommended Shielding Safety Factors

	2 cm gap		4 cm gap	
	Coil	VV	Coil	VV
Assembly gap	1.4	1.9	2.8	6
Modeling	1.6	1.6	1.6	1.6
Nuclear data	1.4	1.4	1.4	1.4
Total	3	4	6	13

V. IMPACT OF MAGNET RADIATION LIMITS ON RADIAL BUILD

Since no well defined magnet radiation limits were provided for ITER, we demonstrated the impact of such limits on the reactor size by performing several one-dimensional calculations. The results implied that there is an immediate need for well defined magnet radiation limits which will have a big impact on how much additional shielding space (if any) is needed which in turn impacts the size of ITER. Any required changes in the major reactor parameters should be made early in the design to reduce impact on the design of the reactor components.

Several magnet radiation limits are still to be determined (TBD) in the General Design Requirements Document (GDRD). A workshop convened at MIT on March 22 and 23, 1993 to propose radiation limits for ITER. It was concluded that the insulator is the most critical component. The fast neutron fluence and insulator gamma dose limits were recommended to be 10^{18} n/cm^2 and 10^9 rads. However, these limits are not officially endorsed by ITER JCT. An insulator dose limit of 10^8 rads, quoted in the GDRD, will be very restrictive. For example, even with an added 10 cm and assuming only a 2 cm assembly gap, the insulator dose will be 5.2×10^8 rads taking into account the 3 safety factor. This implies that at least an increase of 22 cm in blanket thickness is needed. If 4 cm gaps are used, the increase in thickness needed is 27 cm.

The end-of-life insulator dose and neutron fluence are determined by the shielding performance of the breeding blanket used in the EPP which is lower than that of the SS/H_2O shielding blanket used in the BPP. Results of the US blanket trade-off study for ITER indicate that magnet damage is a factor of 4 higher when the CDA breeding blanket is utilized. Hence, an additional space of ~10 cm should be provided for the blanket/shield. It is, therefore, recommended that the inboard space allocated for the blanket/shield should be sized based on the shielding performance of the breeding blanket. The results were presented to the JCT and home teams during the blanket review meeting held in Garching during the period 20-24 February 1995.

VI. NUCLEAR HEATING PROFILE IN TF COILS

At the request of the magnet design group in the US home team, we calculated the nuclear heating profiles in the most recent cased TF coil design. The radial variation of nuclear heating in the inboard and outboard legs of the TF coils are given in Figs. 1 and 2 below with results normalized to unity at the front of the coil case. The nuclear heating drops slowly at the front of the coil (an order of magnitude drop in 35 cm) but drops by an order of magnitude in 20 cm as one moves deeper in the coil. Radial variations are similar in the inboard and outboard legs.

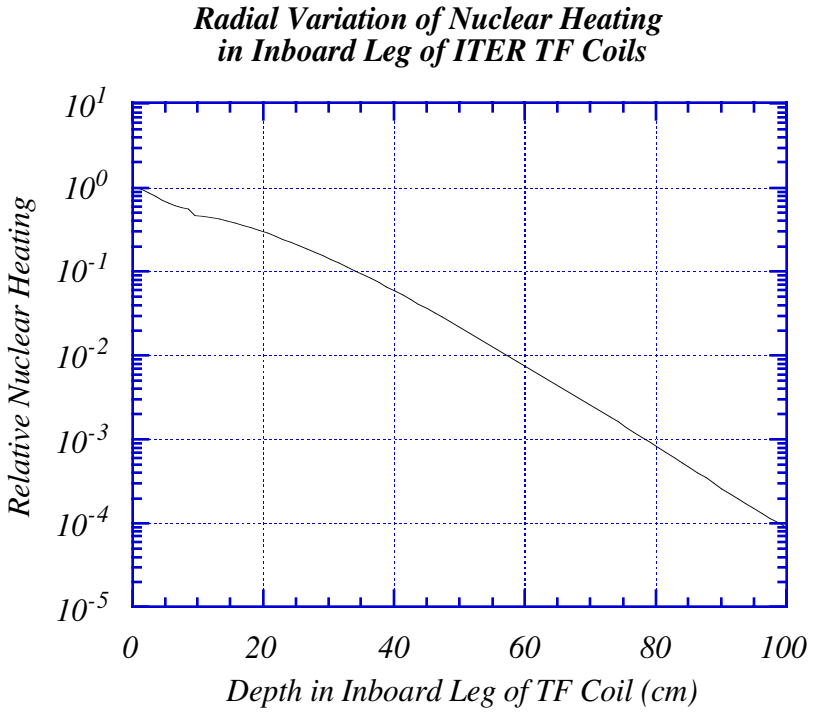

Fig. 1. Radial variation of nuclear heating in inboard leg of TF coils.

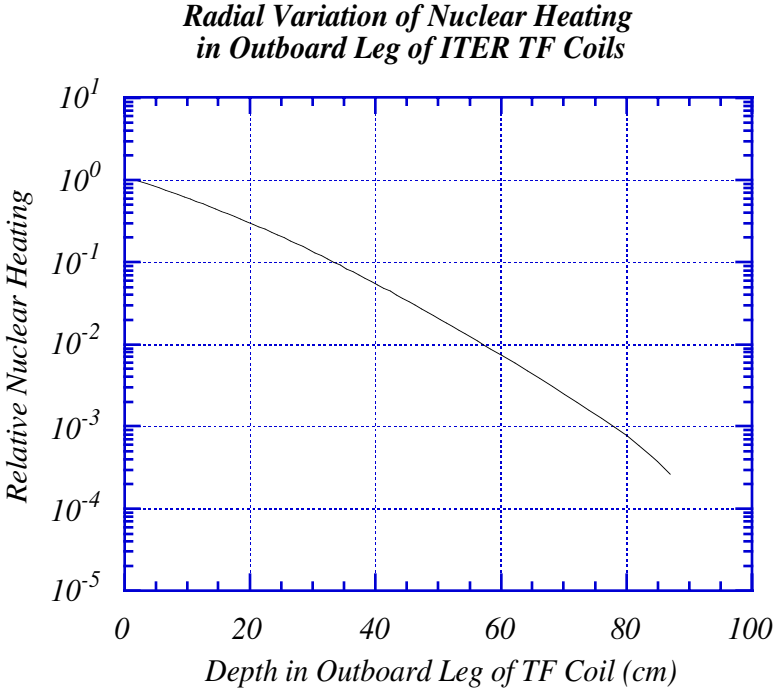

Fig. 2. Radial variation of nuclear heating in outboard leg of TF coils.

VII. ONE- AND TWO-DIMENSIONAL BLANKET NEUTRONICS AND SHIELDING

The University of Wisconsin continued providing support to the JCT Nuclear Analysis group in performing one- and two-dimensional neutronics and shielding calculations for the ITER shielding blanket. We helped the JCT in setting the 1D model and analyzing the results for the shielding blanket, vacuum vessel, and TF coils using the radial build provided by the JCT. Recommendations regarding the vacuum vessel thickness required for adequate magnet protection in the inboard side were made.

One-dimensional radiation transport calculations have been performed to assess the nuclear performance of a shielding blanket-vacuum vessel assembly proposed for use in the 20-toroidal field coil radial build of the ITER. Data were obtained using two different cross-section-nuclear-response data bases to demonstrate differences among calculated results that may arise when the data are processed differently. The main purpose of this study was to determine approximate dimensions of the blanket-vacuum vessel design that maintain acceptable heating and radiation damage response in the magnets and that preserve the recommended radial build at the toroidal magnet midplane. From a neutronics perspective alone, the vacuum vessel thickness can be reduced to ~43 cm and still meet the recommended heat tolerance specifications for the magnet, if the shielding blanket is 42.5 cm thick. The nuclear analysis deals, of course, with only one set of concerns and not with other important effects, such as mechanical stresses, thermal hydraulics, or effects of electromagnetic loads. The actual vacuum vessel dimensions will be determined only after all elements have been adequately evaluated - which will include more detailed two- and three-dimensional radiation transport analyses.

We provided support to the JCT in performing a 2D neutronics calculation to determine the neutron spectrum used for activation calculations to determine the dose rate after shutdown outside the reactor. An R-ϑ model was developed for the design with 20 TF coils. The total of 10,096 (681 x 16) mesh points were modeled. The toroidal variation of magnet damage was clearly demonstrated. The damage parameters were calculated in the outer legs of the TF coils and were found to be in agreement with the 1D results. These damage parameters are about two orders of magnitude lower than those in the inboard leg.

VIII. NUCLEAR HEATING IN AND AROUND ATTACHMENT BOLTS

Neutronics calculations have been performed to determine the nuclear heating distribution in the bolt and surrounding components to be used in the 2D thermal analysis. The nuclear heating values are based on a series of 1D calculations. The values calculated at the first wall for

the different materials (Be, Cu, SS) for unit wall loading were used to determine the nuclear heating at the front surface of the bolt and bolt recess taking into account the effect of the reduction in plasma view factor as one moves deeper in the recess. Based on our calculations for unit wall loading at the outboard FW, the heating values are 16.2, 14.3, and 8.9 W/cm^3 for Cu, SS, and Be using the FENDL library. The wall loading was calculated along the surface in the recess taking into account the plasma view factor. We assumed the worst case for modules above the midplane at z location where the source peaks in the plasma (at magnetic axis). The results were normalized to a peak outboard wall loading of 1.44 MW/m^2. Heating in the bolt was also increased by a safety factor of ~30% to account for uncertainties in estimating the view factor.

IX. NEUTRON WALL LOADING DISTRIBUTION IN THE INTERIM ITER DESIGN

The poloidal distribution of the neutron wall loading in the interim design of ITER has been determined using the three-dimensional radiation transport Monte Carlo code MCNP. The results are normalized to the nominal fusion power of 1500 MW. The detailed geometrical configuration of the ITER first wall and the front surface of the divertor cassette have been modeled in the calculation. In this calculation, only the uncollided neutron current crossing the first wall and the front surface of the divertor cassette is tallied. Hence, the geometrical model includes only the front surface of the first wall and divertor cassette and the plasma chamber zone to reduce the complication for the wall load model.

Output of the MCNP geometry plotting routine is given in Fig. 3. A combination of cones, tori, and cylinders was utilized for accurate modeling of the plasma facing surfaces. The plasma zone is divided into three cells with the scrape-off cell separating them from the first wall. The model used in this analysis utilizes the same surfaces used in the general model developed by D. Valenza of the EU home team at Garching and presented in the Neutronics Working Group Meeting held in Garching in September 1995. However, the cell definition was modified resulting in significant simplification that yields significant savings in computing time. For example the scrape-off cell in the original general model is defined as a complement to the first wall and shield module cells. As a result, about 1700 surfaces define the scrape-off cell. This exceeds the limit of 100 specified in MCNP requiring modification of MCNP to allow for the large number of surfaces per cell. This results also in large computing time since a particle entering a cell has to be checked for crossing all of the surfaces defining the cell. In the simplified cell description the limit on number of surfaces per cell specified in MCNP is not exceeded. The simplification of cell description was performed in collaboration with L. Petrizzi from the EU home team during his stay in Garching as a VHTP.

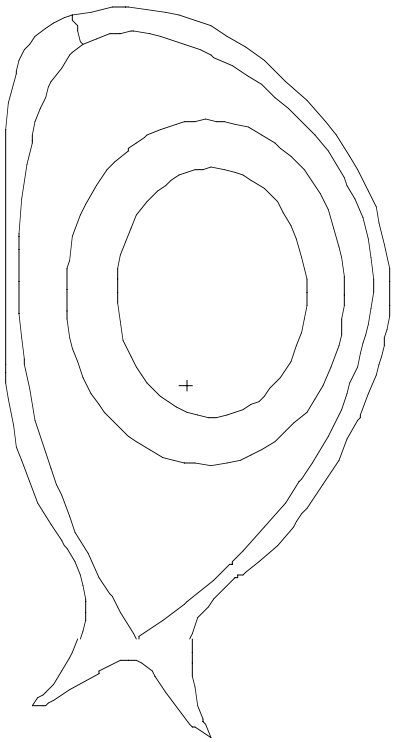

Fig. 3. MCNP model for first wall and plasma facing surface of divertor cassette with plasma region approximated by three cells with uniform source in each of them.

In the original general model developed by D. Valenza, the source neutrons are sampled by determining the cell in the plasma zone in which the neutron is born according to the probability distribution based on the actual source profile. The probabilities assigned to the source cells are 62.5%, 31.25% and 6.25% for the inner, middle, and outer cells, respectively. Once the cell is determined, the source location is determined by sampling uniformly in the cell. Although this is considered a good approximation for the inner cell (plasma core) where the source is flat, the source drops sharply in the outer regions of the plasma. To assess the impact of this approximation on the neutron wall loading distribution, another model was generated for the neutron wall loading calculation. The model is shown in Fig. 4. Only one cell is used to define the plasma chamber where the source is sampled from. A source subroutine has been written to modify MCNP to sample source neutrons from the source distribution in the ITER plasma provided numerically by the San Diego JCT at 1600 mesh points. Two million source particles have been sampled in the MCNP calculation yielding statistical uncertainty less than 0.5% in the calculated wall loading at any first wall segment.

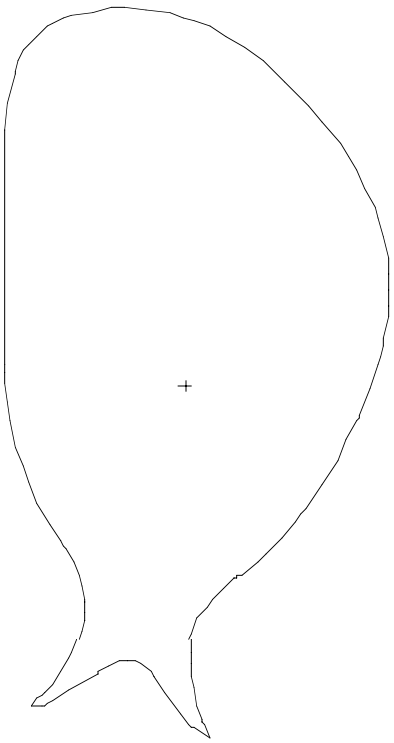

Fig. 4. MCNP model for first wall and plasma facing surface of divertor cassette with plasma region represented by a single cell allowing for source sampling from the exact pointwise source profile.

Source particles travel through void in the plasma chamber until they cross the wall. Particles are killed upon crossing the wall. Surface current tallies have been determined by counting particles crossing the wall. These current tallies represent the neutron wall loading. In order to get the detailed poloidal distribution of the neutron wall loading, the first wall surface has been segmented into 53 poloidal segments and particles crossing each segment have been tallied. The segmentation was done such that the length of each segment is less than 0.5 m. The exact segment areas were calculated analytically. 25 segments were used for the inboard region which includes first wall and shield modules 1 to 7 and 28 segments were used in the outboard region which includes modules 8 to 15. The current crossing the surface at the divertor entrance was also tallied. The plasma facing surface of the divertor cassette has been segmented into 21 poloidal segments to provide the neutron wall loading distribution in the divertor region. The outboard and inboard first wall surface areas are 817.3 and 415 m^2, respectively, and the area at the entrance to the divertor region is 77.7 m^2. The total surface area of the plasma facing surface in the divertor cassette is 293.8 m^2.

Figures 5-7 give the poloidal variation of neutron wall loading in the outboard and inboard regions as a function of toroidal length measured in the clockwise direction from the lower corner of the inboard first wall. Figure 5 shows the results obtained from MCNP with the source sampled from the three cells with uniform distribution. This calculation used a CPU time of 150 min on the Cray computer. Figure 6 gives the poloidal neutron wall loading distribution obtained from MCNP with source sampled from the detailed pointwise source distribution. The CPU time for this calculation is only 115 min. The results are compared in Fig. 7. Figure 8 shows the relative error in neutron wall loading introduced by approximating the source profile by three uniform distributions. The largest difference between the calculated neutron wall loading values in the first wall segments is 11%. The largest errors are in the regions at the bottom and top of the reactor where the neutron wall loading is overestimated. This is due to assuming a uniform source in the outer region of the plasma that results in significant overestimation of the source density at the plasma edge.

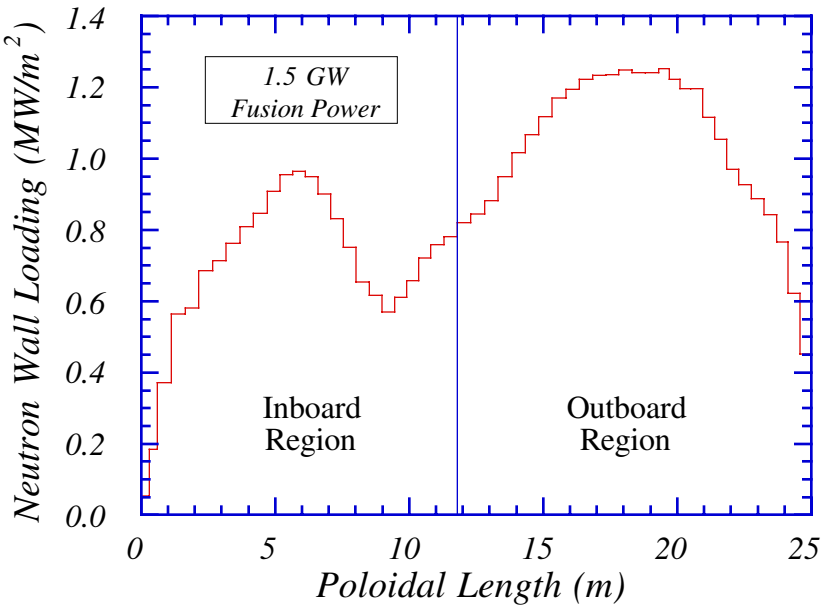

Fig. 5. Poloidal neutron wall loading distribution obtained from MCNP with source sampled from three cells with uniform distribution.

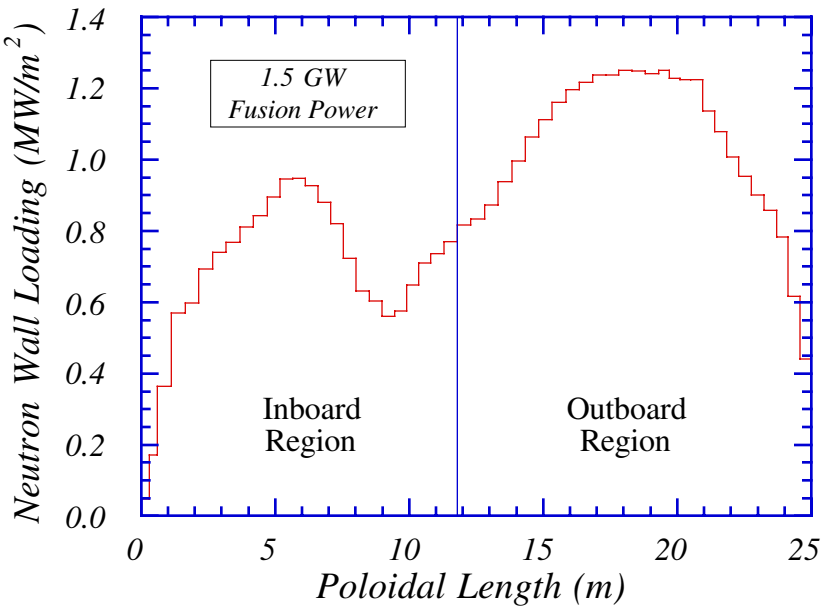

Fig. 6. Poloidal neutron wall loading distribution obtained from MCNP with source sampled from the detailed pointwise source distribution.

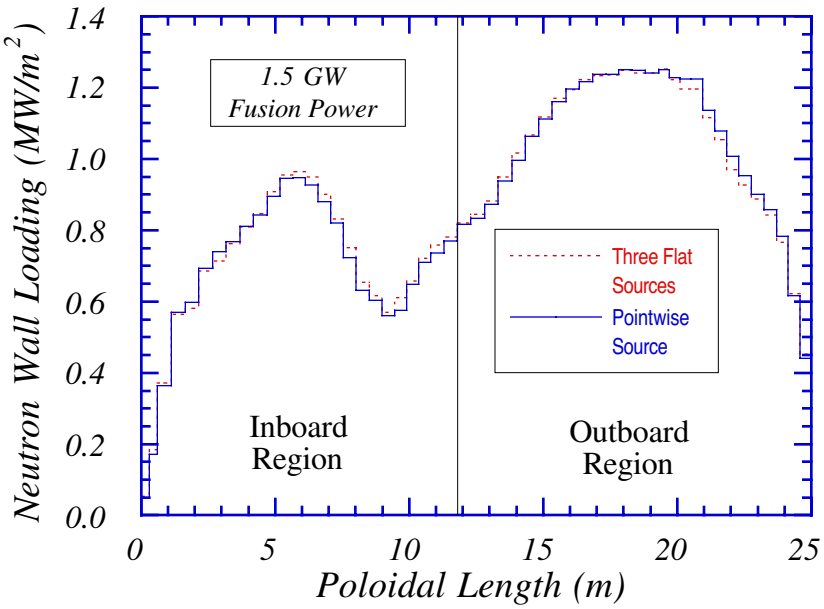

Fig. 7. Poloidal distribution obtained from MCNP with source sampled from three cells with uniform distribution or from the detailed pointwise source distribution.

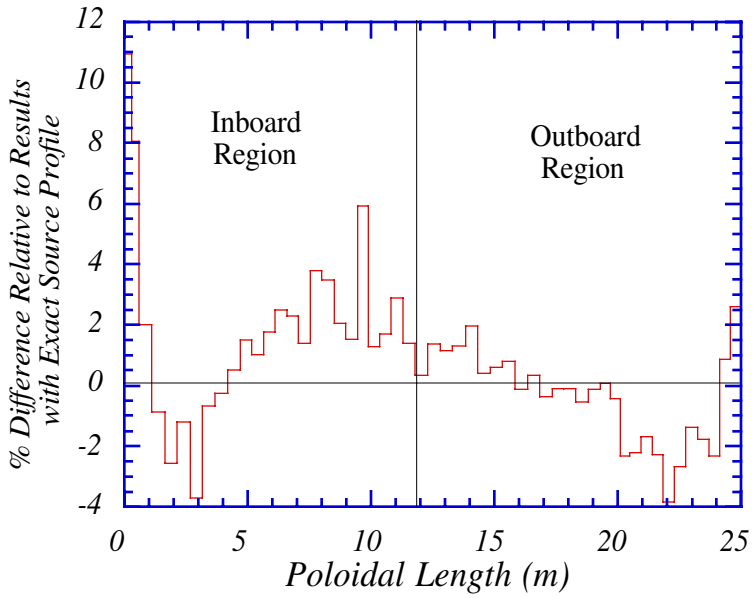

Fig. 8. Relative error in wall loading resulting from sampling the source from three cells with uniform distribution.

Table 4 gives the peak and average neutron wall loading values in the different regions as calculated using the two methods described above. Using the average neutron wall loading values along with the areas of the different regions, one can determine the fraction of source neutrons impinging directly on the different regions. Table 5 gives the fraction of source neutrons going to the inboard, outboard and divertor regions of ITER.

Table 4

Average and Peak Neutron Wall Loading Values (MW/m^2)

	Pointwise Source	Approximate Source
Peak inboard	0.947	0.964
Average inboard	0.685	0.693
Peak outboard	1.250	1.251
Average outboard	1.062	1.058
Average first wall	0.935	0.935
Average divertor entrance	0.606	0.612

Table 5

Fraction of Source Neutrons Impinging Directly on the Different Regions

	Pointwise Source	Approximate Source
Inboard region	23.71%	23.98%
Outboard region	72.37%	72.06%
Divertor region	3.92%	3.96%

Figures 9-11 give the poloidal variation of neutron wall loading in the divertor as a function of toroidal length measured in the counterclockwise direction from the upper corner of the inner vertical target. Figure 9 shows the results obtained from MCNP with the source sampled from the three cells with uniform distribution. Figure 10 gives the poloidal neutron wall loading distribution obtained from MCNP with source sampled from the detailed pointwise source distribution. It is clear that the neutron wall loading peaks in the central dome which has the largest view of the plasma. The neutron wall loading drops as one moves from the central dome along the wings towards the inner and outer vertical targets. The plasma view factor for the inner vertical target is very small resulting in very low neutron wall loading. Table 6 gives the peak and average neutron wall loading values in the different regions of the divertor cassette as calculated using the two methods described above. The average neutron wall loading in the divertor cassette is 0.16 MW/m^2.

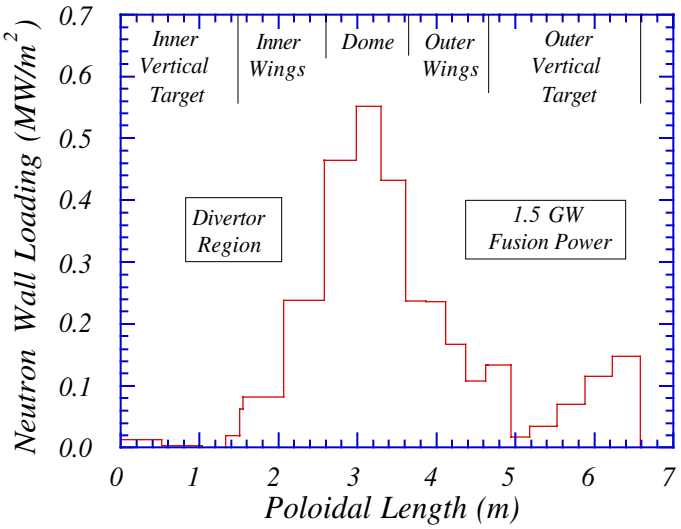

Fig. 9 Poloidal neutron wall loading distribution in divertor obtained from MCNP with source sampled from three cells with uniform distribution.

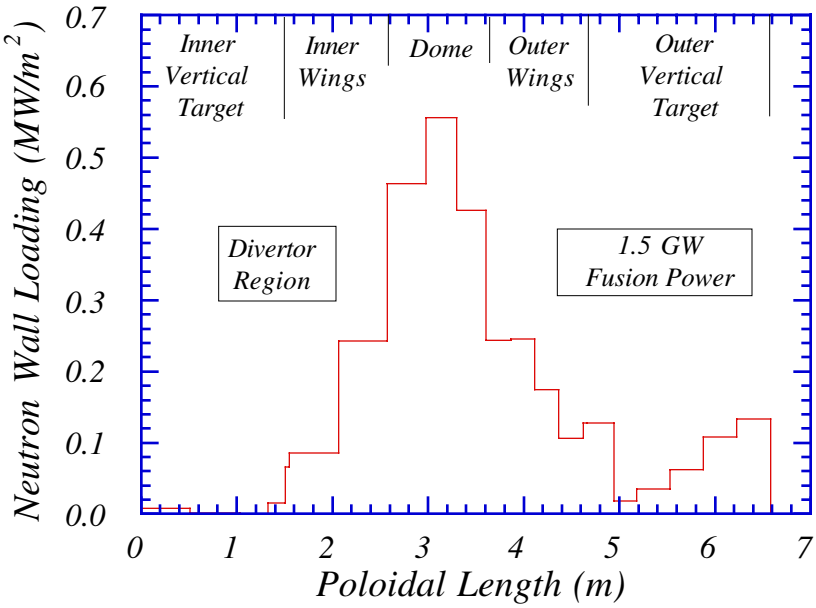

Fig. 10. Poloidal neutron wall loading distribution in divertor obtained from MCNP with source sampled from the detailed pointwise source distribution.

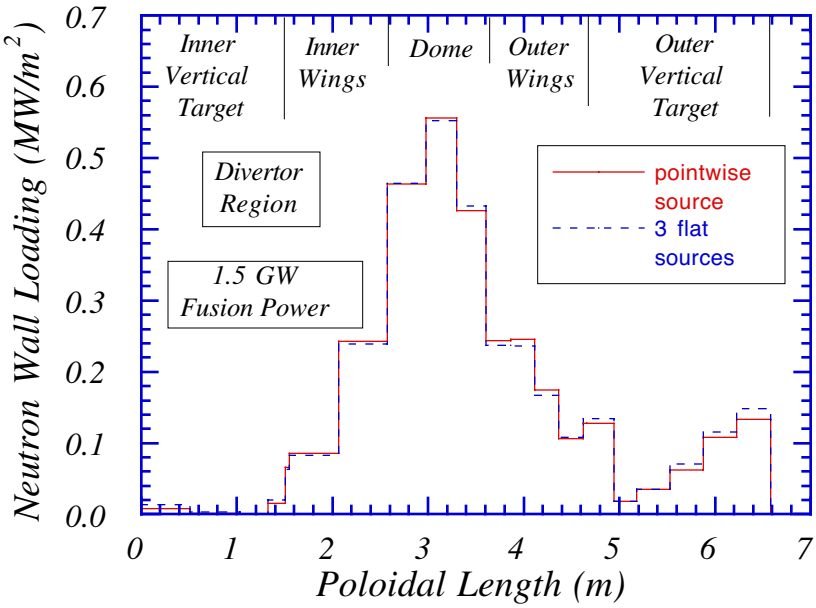

Fig. 11 Poloidal distribution in divertor obtained from MCNP with source sampled from three cells with uniform distribution or from the detailed pointwise source.

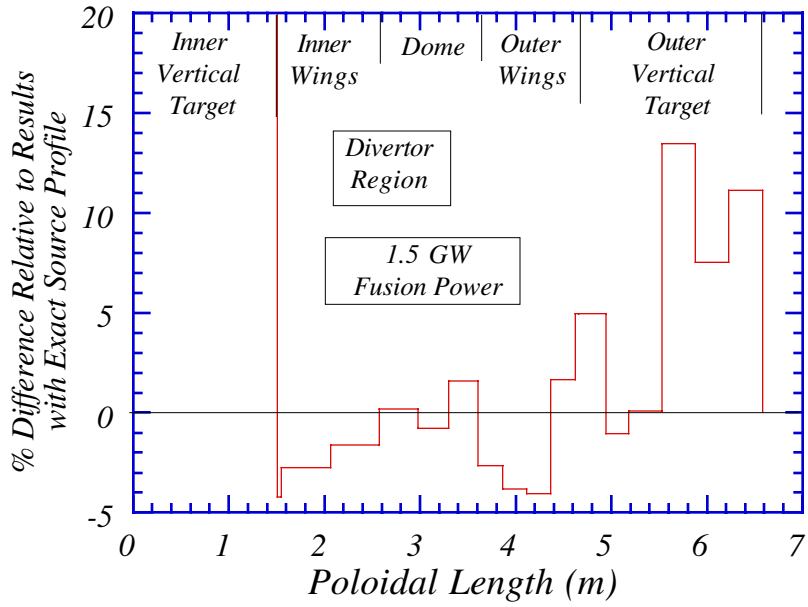

Fig. 12 Relative error in divertor wall loading resulting from sampling the source from three cells with uniform distribution.

Table 6

Average and Peak Neutron Wall Loading Values in the Divertor Cassette (MW/m^2)

	Pointwise Source	Approximate Source
Peak inner vertical target	0.015	0.020
Average inner vertical target	0.007	0.008
Peak inner wings	0.243	0.239
Average inner wings	0.164	0.161
Peak central dome	0.556	0.552
Average central dome	0.481	0.482
Peak outer wings	0.243	0.237
Average outer wings	0.189	0.184
Peak outer vertical target	0.134	0.148
Average outer vertical target	0.083	0.089

The results are compared in Fig. 11. Figure 12 shows the relative error in neutron wall loading introduced by approximating the source profile by three uniform distributions. The difference between the calculated neutron wall loading values in the central dome and inner and outer wings is <5%. However, using three uniform source regions results in overestimating the neutron wall loading by up to 14% in the outer vertical target and up to a factor of 3 in the inner vertical target. Again this is due to assuming a uniform source in the outer region of plasma that results in significant overestimation of the source density at the plasma edge near the plasma null point.

Although the results imply that using the approximate source distribution is not expected to introduce significant errors when used in calculating the neutronics and shielding parameters for the different ITER components, it is recommended using the exact pointwise source with the single plasma chamber cell shown in Fig. 4 which results in shorter computing time. This also makes it straightforward to accommodate any future changes in the source profile by simply replacing the source profile file with the most recent one. The use of the exact source is particularly necessary for calculations in the divertor region. This first wall and plasma chamber model with the source subroutine for sampling from the pointwise source distribution will be integrated in the revised general model under development now in collaboration with L. Petrizzi.

X. PULSED ACTIVATION ANALYSIS

The University of Wisconsin has performed biological dose calculations outside the machine in support of the ITER blanket/shield designs coordinated by the Garching JCT. The radial build provided by the JCT was modeled for a two-dimensional, r and ϑ ($-9° < \vartheta > 9°$) calculation. The total of 8,400 (525×16) mesh points were modeled. All impurities in the FW, blanket, VV, magnet, cryostat and biological shield were included. The calculations were performed for 3 different pulsing scenarios provided to us by the JCT. This included a single pulse (1000 s), 10 pulses (duty factor 50%), and 9470 pulses (duty factor 50%) for a total fluence of 0.3 MW·a/m^2.

The flux was produced using the TWODANT code. The neutron flux is normalized to 1 MW/m^2 wall loading at the outboard. The activation analysis was performed using the DKR-PULSAR1.0 code with cross section data from the USACT93 activation data base. The cross section library used contains data for 3000 nuclides. The gamma source data are based on

ENDF/B-VI. The gamma library contains data for 1788 nuclides. The gamma source from decay was determined at all mesh points and transported, using the TWODANT code, to calculate dose rate at different locations following shutdown. The dose rates were calculated as a function of toroidal angles at locations in the space between the TF coils and cryostat, and in the space between the cryostat and the biological shield. An inter-coil mechanical support was included in the space between coils. The dose rates were calculated as a function of toroidal angle at locations shadowed by the magnet and in the space between magnets. Finally, a set of 1-D calculations was performed for the purpose of comparing their results to results obtained from the 2-D analysis.

As shown in Figures 13-22, the 2-D results clearly showed the toroidal effect which is dominated by contribution from the activation of the cryostat and the biological shield. After one pulse, full access to the machine is possible within a few hours following shutdown. After 10 pulses, full access is also possible within the first day following shutdown. At the end of the Basic Performance Phase, full access is possible at any of the locations considered after one week following shutdown. Adding the inter-coil mechanical support provided more shield behind the V.V. resulting in a reduction of the biological dose rate (1 day following shutdown) by a factor of five when compared to previous two-dimensional calculations that did not include the inter-coil structure.

As shown in Tables 7 and 8 comparison between one-dimensional and two-dimensional calculations showed that using 1-D results in significant underestimation of the biological dose rates behind the TFC. On the other hand, 1-D results are about 50% higher than the 2-D results in areas shadowed by the inter-coil structure. As shown in Figures 23-26, adding a 1 cm-thick layer of boron to the front of the biological shield resulted in reducing the dose at locations between the coils and cryostat by 65% due to the reduction in thermal neutron capture in the concrete. On the other hand, adding the boron layer resulted in the reduction of the dose between the cryostat and biological shield by a factor of three.

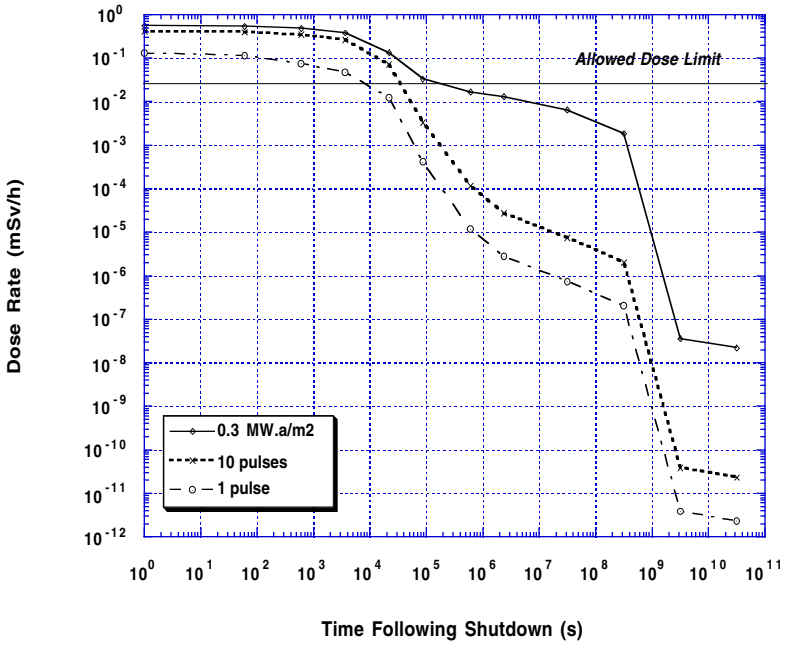

Fig. 13. Biological dose rates behind TFC (in the shadow of TFC) as a function of time following shutdown.

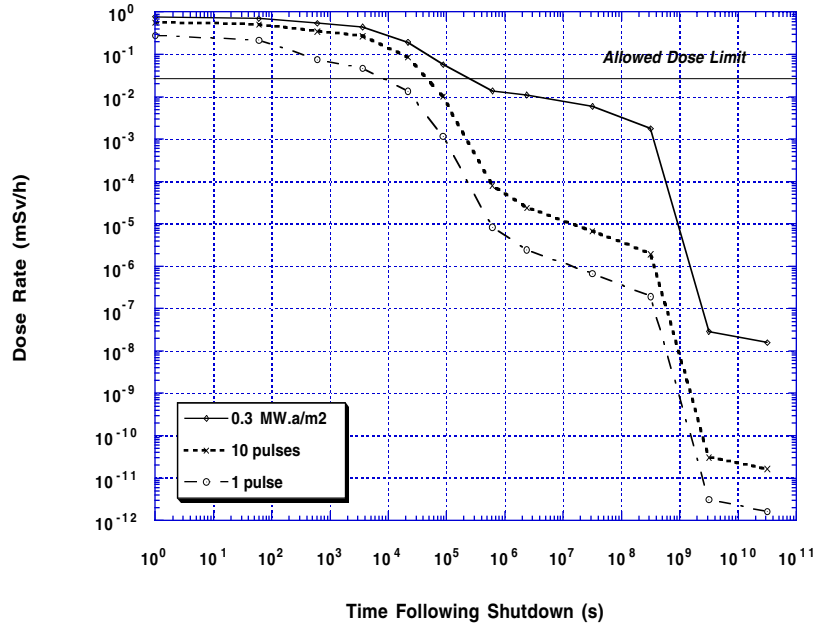

Fig. 14. Biological dose rates behind cryostat (in the shadow of TFC) as a function of time following shutdown.

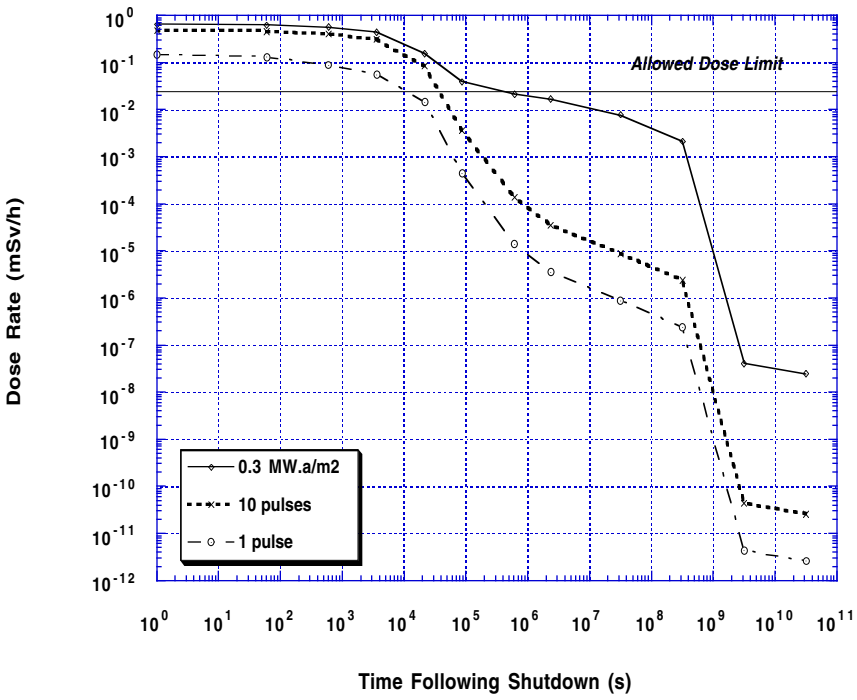

Fig. 15. Biological dose rates behind TFC (in the shadow of inter-coils) as a function of time following shutdown.

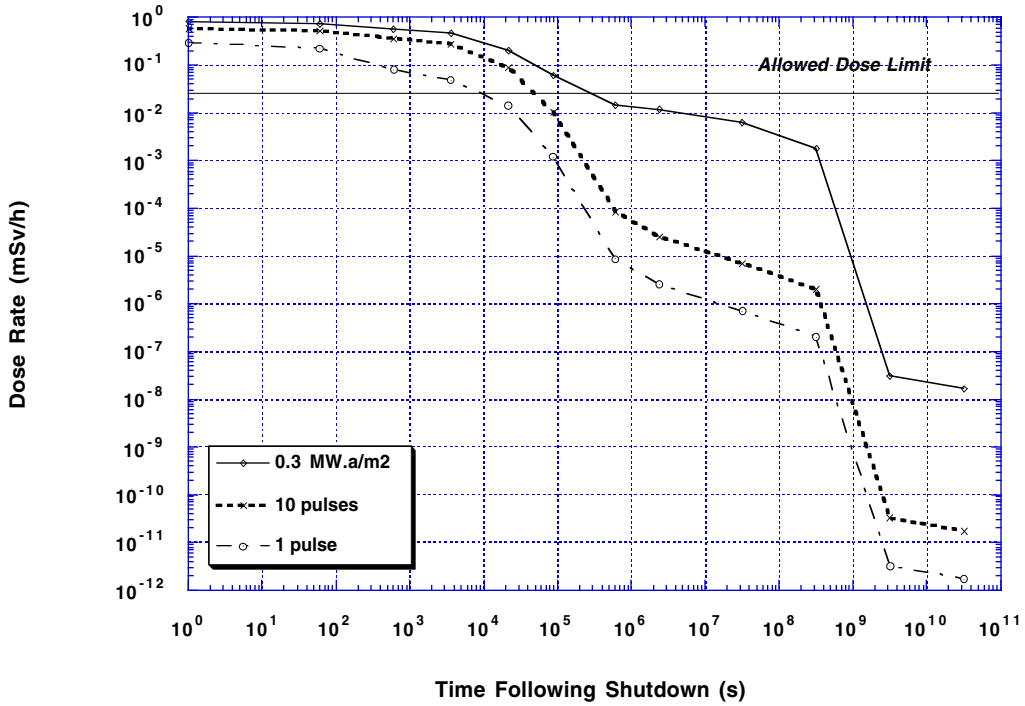

Fig. 16. Biological dose rates behind cryostat (in the shadow of inter-coils) as a function of time following shutdown.

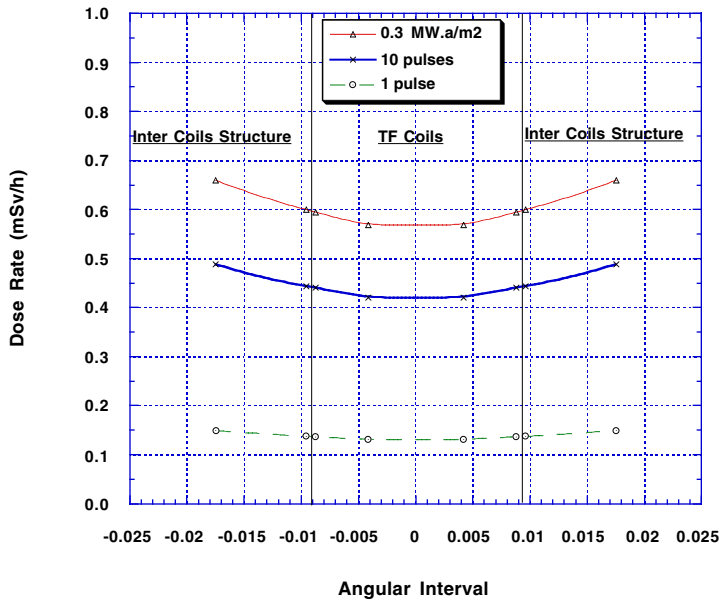

Fig. 17. Biological dose rates behind TFC at shutdown and as a function of angular interval.

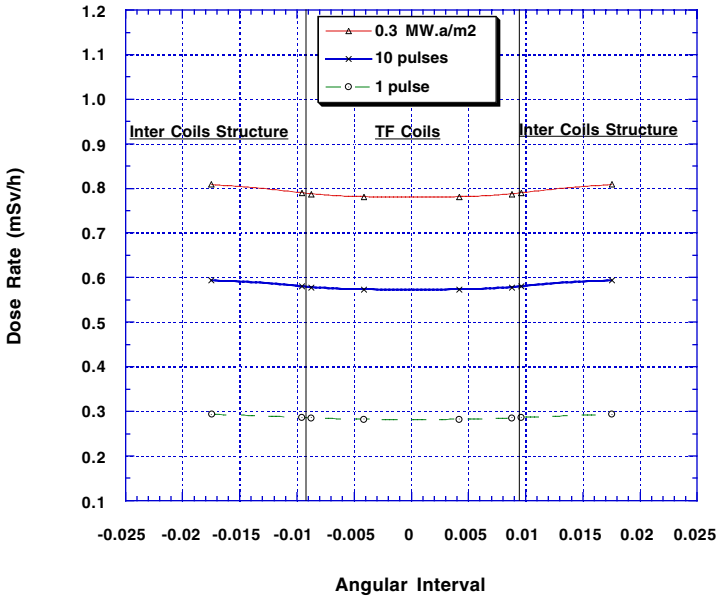

Fig. 18. Biological dose rates behind cryostat at shutdown and as a function of angular interval.

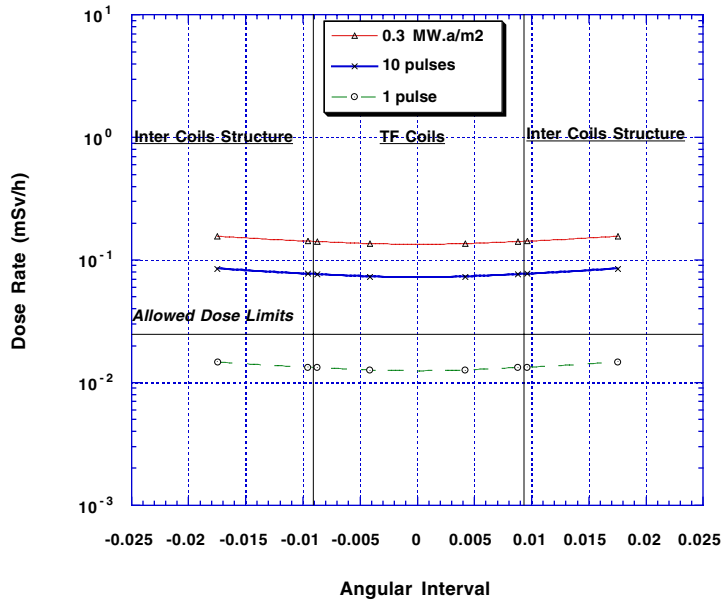

Fig. 19. Biological dose rates behind TFC at 6 hr and as a function of angular interval.

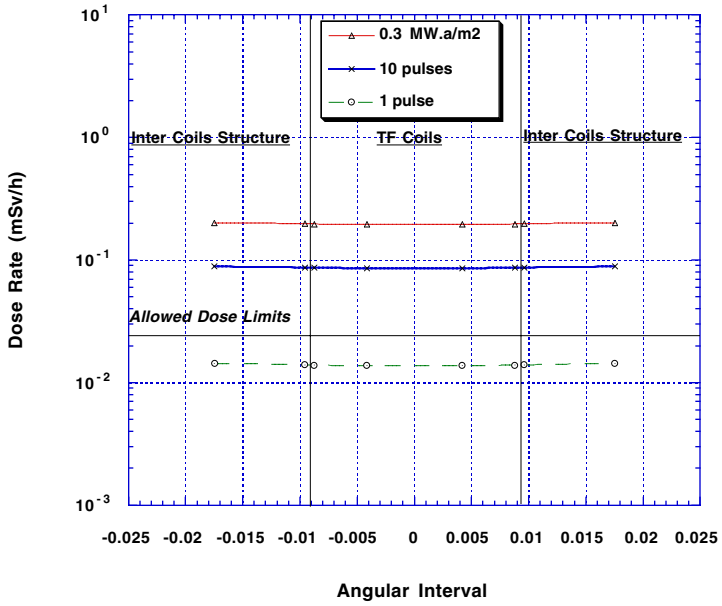

Fig. 20. Biological dose rates behind cryostat at 6 hr and as a function of angular interval.

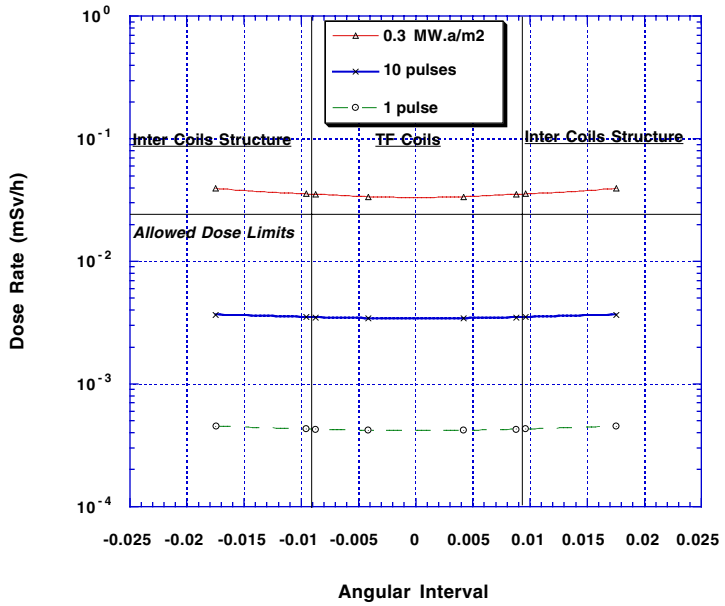

Fig. 21. Biological dose rates behind TFC at 1 day and as a function of angular interval.

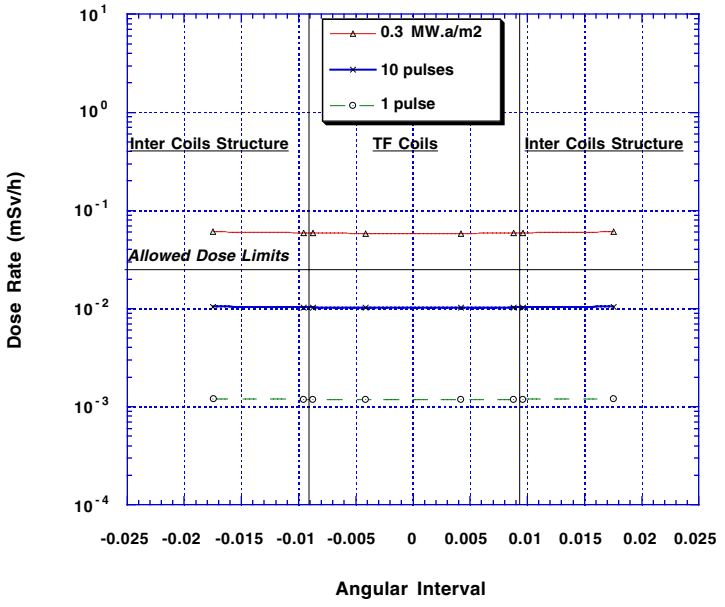

Fig. 22. Biological dose rates behind cryostat at 1 day and as a function of angular interval.

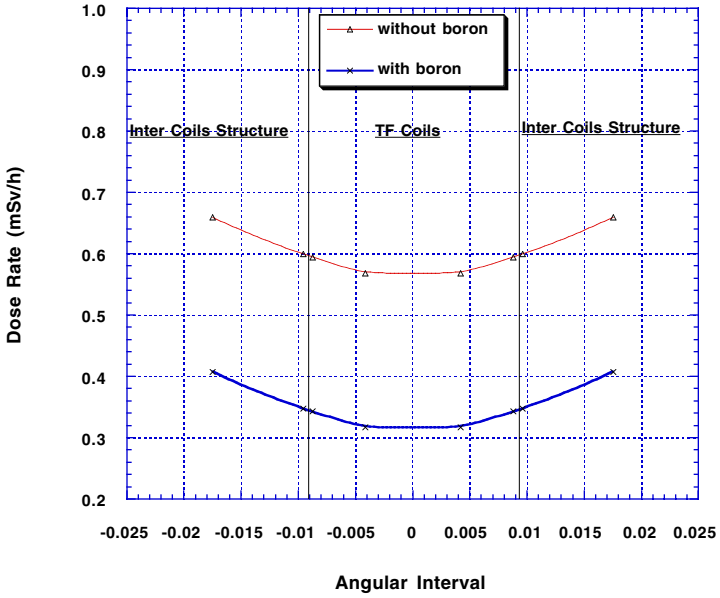

Fig. 23. Impact of adding a 1 cm layer of boron to the inner surface of the biological shield on dose rates behind TFC at shutdown.

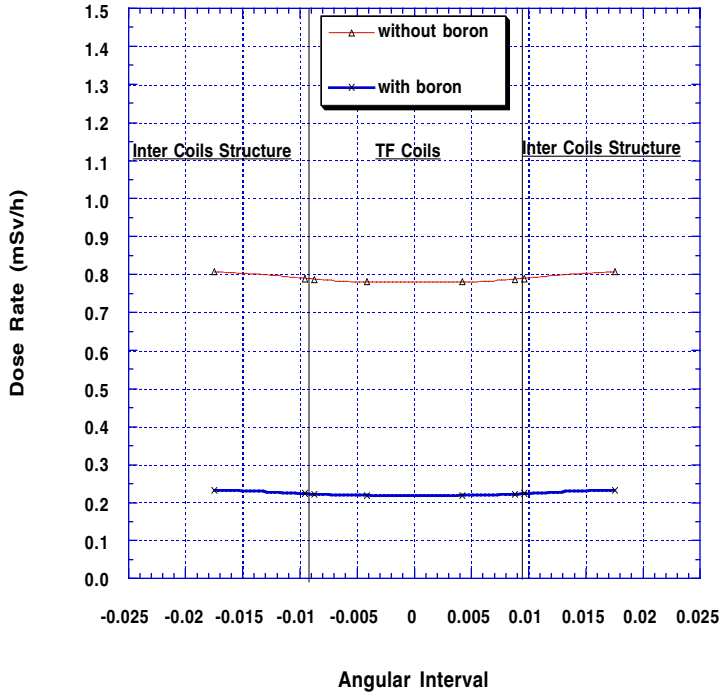

Fig. 24. Impact of adding a 1 cm layer of boron to the inner surface of the biological shield on dose rates behind cryostat at shutdown.

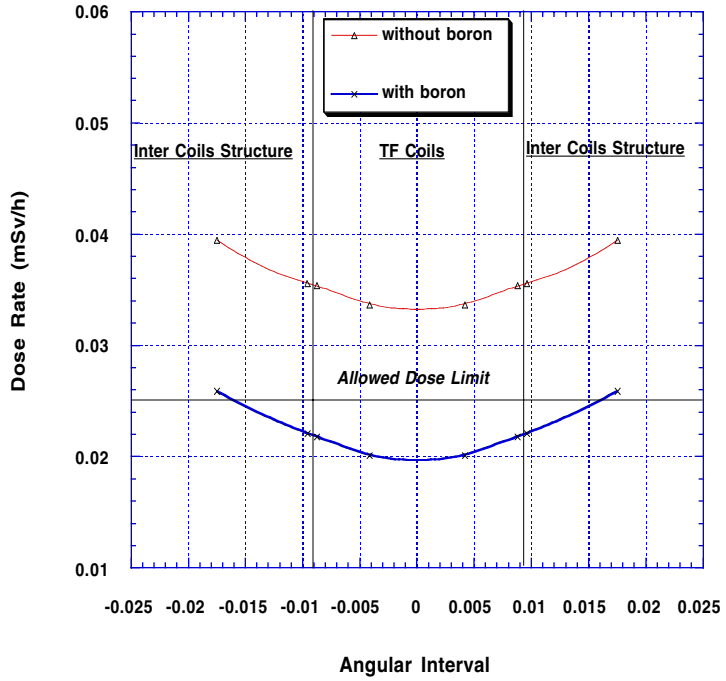

Fig. 25. Impact of adding a 1 cm layer of boron to the inner surface of the biological shield on dose rates behind TFC 1 day after shutdown.

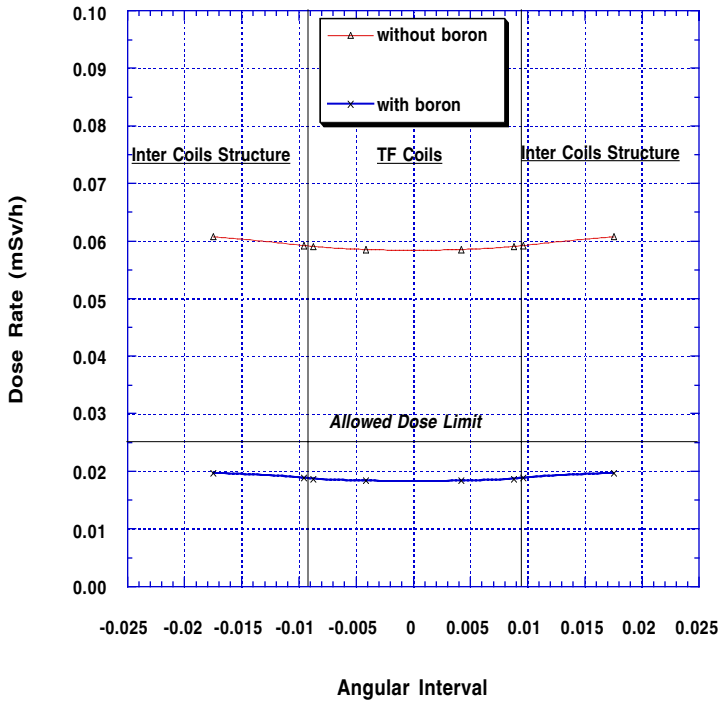

Fig. 26. Impact of adding a 1 cm layer of boron to the inner surface of the biological shield on dose rates behind cryostat 1 day after shutdown.

Table 7

2-D vs. 1-D

Method	Location	Dose (mSv/hr)	Dominant Nuclides	Source of Nuclides
2-D	between coils and cryostat (coils shadow)	0.0337	(1) ^{24}Na (29%) (2) ^{60}Co (21%)	bio-shield (100%) cryostat (53%) inter-coils (24%) TFC (17%)
1-D	between coils and cryostat (coils shadow)	1.53e-7	(1) ^{24}Na (23%) (2) ^{60}Co (21%) (3) ^{99}Mo (21%)	bio-shield (100%) TFC (52%) cryostat (43%) TFC (56%) cryostat (44%)
2-D	between coils and cryostat	0.0395	(1) ^{24}Na (25%) (2) ^{60}Co (21%) (3) ^{58}Co (15%)	bio-shield (100%) cryostat (45%) inter-coils (45%) TFC (5%) inter-coils (69%) cryostat (30%)
1-D	between coils and cryostat	0.0555	(1) ^{24}Na (27%) (2) ^{60}Co (22%) (3) ^{99}Mo (15%)	bio-shield (100%) cryostat (49%) inter-coils (46%) inter-coils (52%) cryostat (47%)
2-D	between cryostat and bio-shield (coils shadow)	0.0586	(1) ^{24}Na (69%) (2) ^{60}Co (11%)	bio-shield (100%) cryostat (63%) bio-shield (29%)
1-D	between cryostat and bio-shield (coils shadow)	2.3e-7	(1) ^{24}Na (65%) (2) ^{60}Co (12%)	bio-shield (100%) cryostat (62%) bio-shield (27%) TFC (10%)
2-D	between cryostat and bio-shield	0.0608	(1) ^{24}Na (68%) (2) ^{60}Co (11%)	bio-shield (100%) cryostat (63%) bio-shield (29%)
1-D	between cryostat and bio-shield	0.0928	(1) ^{24}Na (69%) (2) ^{60}Co (12%) (3) ^{59}Fe (6%)	bio-shield (100%) cryostat (63%) bio-shield (29%) inter-coils (8%) cryostat (65%) bio-shield (27%) inter-coils (8%)

Table 8

The Impact of Adding a Layer of Boron to the Biological Shield

Method	Location	Dose (mSv/hr)	Dominant Nuclides	Source of Nuclides
2-D (w/o boron)	between coils and cryostat	0.0395	(1) ^{24}Na (25%)	bio-shield (100%)
			(2) ^{60}Co (21%)	cryostat (45%) inter-coils (45%) TFC (5%)
			(3) ^{58}Co (15%)	inter-coils (69%) cryostat (30%)
2-D (w boron)	between coils and cryostat	0.0259	(1) ^{58}Co (22%)	inter-coils (69%) TFC (11%)
			(2) ^{60}Co (19%)	inter-coils (62%) cryostat (30%)
			(3) ^{99}Mo (18%)	inter-coils (57%) cryostat (37%)
2-D (w/o boron)	between cryostat and bio-shield	0.0608	(1) ^{24}Na (68%)	bio-shield (100%)
			(2) ^{60}Co (11%)	cryostat (63%) bio-shield (29%)
2-D (w boron)	between cryostat and bio-shield	0.0197	(1) ^{24}Na (63%)	bio-shield (100%)
			(2) ^{60}Co (9%)	cryostat (45%) bio-shield (30%)

XI. SUMMARY

Two multigroup working libraries were generated based on the most recent FENDL nuclear data evaluation. These libraries were used by the JCT in neutronics calculations. Several neutronics calculations were performed in the early stage of the ITER interim design to provide guidance for the blanket design regarding the impact of blanket thickness on magnet radiation effects and vacuum vessel helium production. We provided a recommended set of safety factors that need to be applied to the one-dimensional results in the early stages of the design to account for gaps between adjacent blanket modules and uncertainties in modeling and nuclear data. Since no well defined magnet radiation limits were provided for ITER early in the year, we demonstrated the impact of such limits on the reactor size by performing several one-dimensional calculations. The results implied that there is an immediate need for well defined magnet radiation limits.

At the request of the magnet design group in the US home team, we calculated the nuclear heating profiles in the most recent cased TF coil design. We continued providing support to the

JCT Nuclear Analysis group in performing one- and two-dimensional neutronics and shielding calculations for the ITER shielding blanket. Recommendations regarding the vacuum vessel thickness required for adequate magnet protection in the inboard side were made. Neutronics calculations have been performed to determine the nuclear heating distribution in the bolt and surrounding components to be used in the 2D thermal analysis.

The poloidal distribution of the neutron wall loading in the interim design of ITER has been determined using the 3D radiation transport Monte Carlo code MCNP. The detailed geometrical configuration of the ITER first wall and the plasma facing surface of the divertor cassette has been modeled in the calculation. The MCNP code was modified to sample source neutrons from the pointwise source distribution in the ITER plasma provided numerically by the San Diego JCT at 1600 mesh points. The peak inboard and outboard wall loadings are 0.95 and 1.25 MW/m^2, respectively. The peak neutron wall loading in the divertor cassette are 0.556 and 0.16 MW/m^2, respectively.

Two-dimensional activation calculations have been performed to calculate the biological dose outside the machine. The detailed radial build at the reactor midplane as provided by the JCT was included in the model. The R-J model used includes 10,096 mesh points. All impurities in the FW, blanket, VV and magnet were included. The calculations were performed for different pulsing scenarios provided by the JCT. The 2D activation calculation has been updated to include the inter-coil structure, cryostat and biological shield. The effect of adding these components in the model was to reduce the dose after shutdown in the space between the vacuum vessel and the cryostat by a factor of ~5. Recommendations regarding accessibility for maintenance in the area behind the VV, TF coils, and cryostat were made.